# NANOSTRUCTURED TI-C THIN FILMS DEPOSITED BY THERMIONIC VACUUM ARC (TVA) TECHNOLOGY

V. Ciupina[1,2], R. Vladoiu[1,2], C. P. Lungu[3], C. Porosnicu[3], G. C. Prodan[1], E. Vasile[4], A. Mandes[1], V. Dinca[1]. A. Velea[5], V. Nicolescu[6]

[1]Ovidius University of Constanta, 124 Mamaia Avenue, Constanta, Constanta, Romania 900527

[2]Academy of Romanian Scientists, Splaiul Independentei No. 54, Bucharest 050094, Romania

[3]National Institute for Lasers, Plasma and Radiation Physics, P.O. Box MG-36, 077125 Bucharest Romania

[4]University Politehnica of Bucharest, Faculty of Applied Chemistry and Material Science, Department of Oxide Materials and Nanomaterials, No. 1–7 Gh. Polizu Street, Bucharest 011061, Romania

[5]National Institute for Materials Physics, Atomistilor No. 405, 077125, Magurele, Romania

[6]CERONAV Constanta, Pescarilor Street no. 69A, 900581 Constanta, Romania

**Abstract.** Nanostructured titanium-carbon nanostructured thin films were prepared using the Thermionic Vacuum Arc (TVA) technology in different configurations under a varied number of Ti/C combinations at high base pressure of $1 \times 10^{-6}$Torr with and without graded compositions. The layers consisting of about 100nm Carbon base layer and seven 40nm alternatively Ti and C layers were deposited on Silicon substrates. On the other hand, in order to obtain C-Ti multilayer structures with variable thickness and different percentages in C and Ti of layers, a 20nm thick C layer was first deposed on Si substrate and then seven Ti-C layers, each of these having thickness of up to 40nm were deposed. To perform the successively layers with various thickness were changed the discharge parameters for C and Ti plasma sources to obtain the desirable thickness. By changing of substrate temperature between room temperature and 300°C and on the other hand the bias voltage up to -700V, different batches of samples were obtained for this study. The films were characterized by surface morphology, and microstructure, through Rutherford Backscattering Spectrometry (RBS), Raman Spectroscopy, Transmission Electron Microscopy (TEM), Grazing Incidence X-ray diffraction (GIXRD). Tribological and electrical measurements are also presented.

**Keywords**: TVA, C–Ti multilayer, EDX, XPS, tribological properties, electrical properties, TEM, STEM

**DOI https://doi.org/10.56082/annalsarsciphyschem.2022.1.107**

## 1. Introduction

Titanium and carbon have outstanding properties that have led to their widespread use in several important technological applications. For instance, with the highest strength-to-density ratio of any metallic element and due to its high corrosion resistance, titanium is used as bulk or coating in propeller shafts,

rigging, and other parts of boats that are exposed to seawater or a salty environment. [1]

However, one of the main drawbacks of titanium is the difficulty in producing a reliable and strong joint due to a lack of metallurgical compatibility and the formation of intermetallic compounds (IMCs) between the two materials. This shortcoming can be surpassed by using Ti-based composites, thereby producing a highly reliable joint structure. [2] For instance, Ti embedded in a carbon (C) matrix could improve adherence of the coated substrates to obtain better hardness and anticorrosive properties [3].

This is why the relationship between structural and mechanical properties of nanocrystalline TiC/amorphous C thin films had increased a great interest. Moreover, the average size of TiC crystallites and the thickness of the carbon matrix should be correlated with Ti content in the films.

Many methods for obtaining titanium-carbon nanocomposites (TiCx/a-C) with or withour graded composition have been studied during the last years, including: Chemical Vapor Deposition (CVD), Physical Vapor Deposition (PVD), Magneton Sputtering.

The major interest from the point of view of properties of Carbon-Titanium nanostructures aims to obtain the dominant TiC phase in such nanostructures.

In reference [4] is examined the formation of Titanium carbide and Titanium phases and their influence on the mechanical properties in the case of some thin films layers. Such structures are deposited by DC magnetron sputtering at room temperature in ultrahigh vacuum from Carbon and Titanium targets. Cubic Titanium carbide phase is formed from 58 to 86 at. % Titanium content. Dominance of cubic Titanium carbide texture with increasing of Titanium content is observed.

A discussion about amorphous carbon and titanium-carbon nanocomposite ($TiC_x$/a-C) coatings deposited by PVD method is given in reference [5]. In this case $TiC_x$/a-C is obtained by simultaneous sputtering of grafite and titanium targets using arc pulse and arc sputtering respectivelly. It is notised that the incorporation of Ti ions into thhe plasma flow of C increases the number of $sp^2$ bonds in carbon matrix of $TiC_x$/a-C, as compared to a-C deposited under similar conditions.

In reference [6] is studied the effect of synthesis conditions on the formation of titanium carbide phase on silicon surfaces by DC magnetron ion-plasma sputtering of combined graphite/titanium target. The X-ray diffraction analysis and Raman spectroscopy showed that the structure of titanuium carbide films depend on the substrate temperature. Gaussian decomposition of Raman spectra

revealed the changes in vibrational modes presumably induced by changes in $Ti_xC_y$ lattice parameters.

The formation of TiC and Ti phases and their influence on their mechanical properties was studied in reference [7]. Thin layeers were deposited by DC magnetron sputtering at room temperature in ultrahigh vacuum from Ti and C targets. Dominance of c-TiC(111) texture with increasing Ti content was observed.

The authors of reference [8] presented Titanium/Diamond like carbon bilayer films with different relative thickness which were synthesized by direct current and pulsed cathode arc plasma method. The studies show the microstructure evolution with varying the thicknesses of Ti interlayer and Diamond like carbon layer. The results are associated with the occurrence of atomic diffusion process at Ti/C interface.

The content of paper [9] refers to C-Ti films prepared on n-type silicon wafers by reactive sputtering , which is the combination of radiofrequency plasma enhanced chemical vapor deposition and sputtering. Pure methane is used as the precursors gas to form the amorphous carbon film. Argon is used as the sputtering gas to bombard the titanium target surface in order to dope titanium in amorphous carbon films by sputtering. The C-Ti film changes from semiconductor character to conductor character when the radiofrequency power increase from 50W to 350W having a rectifying behavior.

In the past decades many efforts have been made on carbon-titanium nanocomposites to improve tribological behavior. Thus, the data contained in paper [10] are related to the technology of salt bath carburizing at low temperature used to prepare the titanium carbide thin film on Ti6Al4V alloy surface. The processed alloy significally improves the friction properties of the structures, based on phase carbide $Ti_8C_5$ generated on the surface of the structure.

In reference [11] the authors aimed the thermal dependence of mechanical properties and structure of nanocomposites of TiC/a-C:H deposited on steel substrates by unbalanced reactive magnetron sputtering of titanium in an active acetylene containing atmosphere. The as-deposited coatings show low friction coefficient.

In reference [12] the authors present some hard multilayer coatiings with a systematic alternation of the pair [($TiC_x$/Ti/C)+(a-C))] deposited on stainless and tool steel by PVD technique. The specific coefficient of nanofrictional wear of such coatings with different compositions of titanium containing layers is determined.

The microsctructure and chemical composition of the Ti-doped anorphoys carbon multilayer films with different Ti content are presented in reference [13]. Such multilayer films are deposed on medical Ti6Al4V alloy using a closed field unhanced magnetron sputtering. Evaluating the mechanical and tribological properties was found that the titanium content has a significant influence on these properties. Thus, these films displays high hardness and low friction coefficient.

The authors of refernece [14] present Titanium/diamond-like carbon multilayeer films deposed using a hybrid system combining radio frequeny sputtering and radio frequency-plasma enhanced vapor deposition (PECVD) techniques under a varied number Ti/diamond-like carbon bilayers. The multilayer approach was used to create unique structures such as nanospheres and nanorods on films. These films were found to have excelent nanomechanical properties.

In reference [15] the authors present Ti-doped diamond-like carbon nanocomposite thin films with different Ti contents prepared by closed field enhanced magnetron sputtering. The measurements confirm the presence of nano-TiC phases and amorphous carbon. The film with a Ti target current of 0.3A exibits the lowest the friction coefficient of 0.02.

The study [16] is focused on the difference in tribological properties and fracture of the coatings which are designed using two different types of magnetron sputtering technology: high power impulse (pulsed) and direct current (non pulsed). Was included friction test before and after fraction.

In reference [17] the study is targeted on the analysis of the surface geometry and elastic properties of carbon based coatings, which are deposed using a high power impulse and direct current migration current magnetron sputtering. The work include friction tests microscopic study of the samples surface, before and after friction.

The aim of this work is to review the behavior of multiple composite Ti and C films that could allow their optimization for advanced engineering applications by using TVA technology, in different configurations and algorithm of deposition with and without graded compositions. This system combines the advantages associated with vacuum techniques and the relatively high rate of deposition, especially the ease in tailoring film composition by controlling the input arc power.

Thermionic Vacuum Arc (TVA) is a versatile method, especially suitable for processing refractory metals, e.g. carbon or tungsten, however, in the course of time various useful applications of this system originated. [18] They include

layers for fusion application, hard coatings, low-friction coatings, biomedical-applicable films, materials for optoelectronics and for solid-state batteries. [19-24]

The purpose of our work is to fabricate C-Ti multilayer nanostructures with certain mechanical and electrical properties determined by the content of $Ti_xC_y$ and Ti phases Such nanostructures are relatively easy to obtain being essentially aletrnative layers of C and Ti deposited on the Si substrate at different temperature and bias voltages. The aim was highlight the $Ti_xC_y$ and Ti phases by Raman measurements and electron microscopy as well as by coefficient of friction and electrical conductivity measurements. Such structures can have various applications due to the possibility of changing the friction coefficient as well as due to the feasibility of switching from the semiconductor character to the metallic character and implcitly changing the sign of the coefficient of variation of the electrical resistance with temperature.

## 2. Experimental set-up

In order to obtain high quality C-Ti multilayer thin films on Silicon substrates was used Thermionic Vacuum Arc (TVA) method [25]. The experimental set-up (Fig.1) consist by two independent anode-cathode systems fixed inside the deposition chamber. Anode was represented by the coating material and the cathode by an electron thermoemissive red-hot tungsten wire. The Ti layers were obtained by placing the bulk material into thermos-resistant $TiB_2$ crucible and heating it until a constant vapor pressure is achieved; by increasing the high voltage applied on the material, a plasma is generated in its vapors. In this case the layers are obtained with both neutrals and ions coming from the Ti plasma source. Due to the fact that C doesn't melts but sublimates at very high temperatures (3650°C) it was deposited from a circular rod. The coating process started upon reached $10^{-6}$torr pressure inside the reaction chamber. In a first way of working, the coated films (samples ***A1,A2,*** etc.), consisted of a base layer of about 100nm thick carbon deposited at low evaporation rates in order to ensure its stability on the substrate. Subsequently, seven carbon and titanium layers were deposited alternatively on top of carbon base layer, each of them has a final thickness up to 40nm.

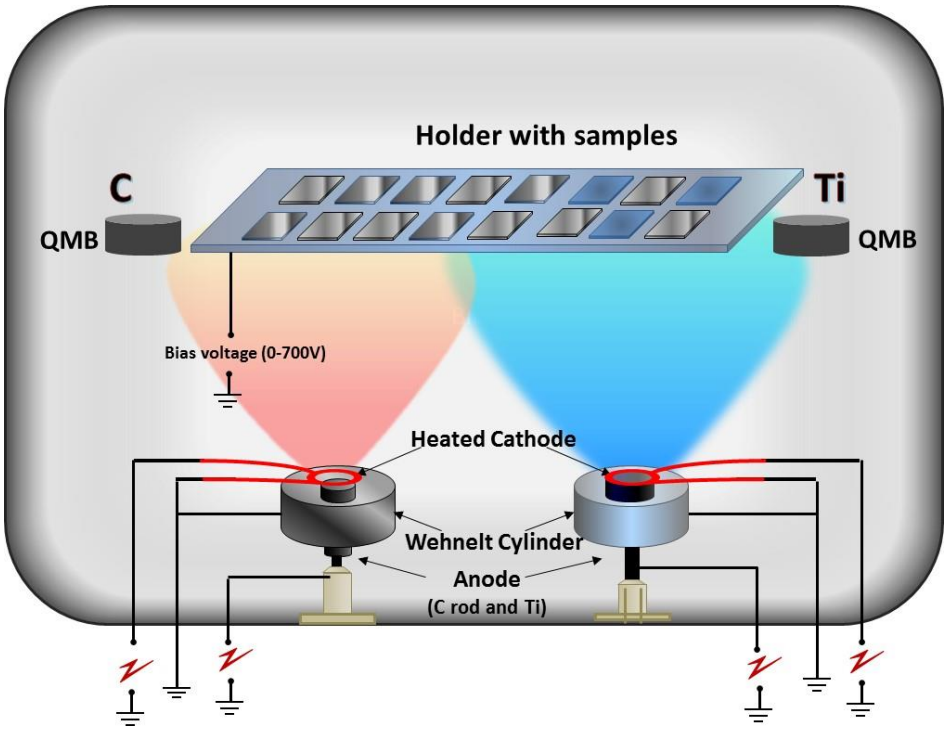


**Figure 1.** The schematic view of the experimental set-up

C/Ti layer distribution is shown in Fig.2. The differnce of the various A samples is due to relative position of the substrates fixed in the holder with respect to the two plasma sources of carbon and titanium (Fig. 3.). In a secod way of working the coated films (samples ***B1,B2,***etc.) consisted of a carbon base layer having a thickness of about 20nm and seven carbon-titanium layers , each having a thickness of 40nm.

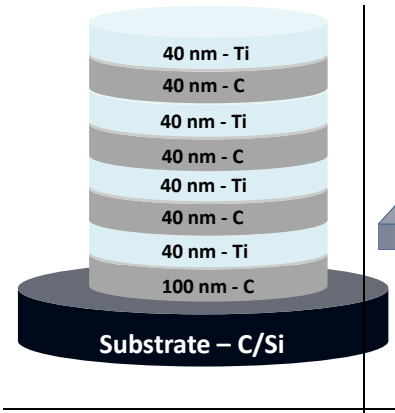


**Figure 2.** C/Ti layer distribution

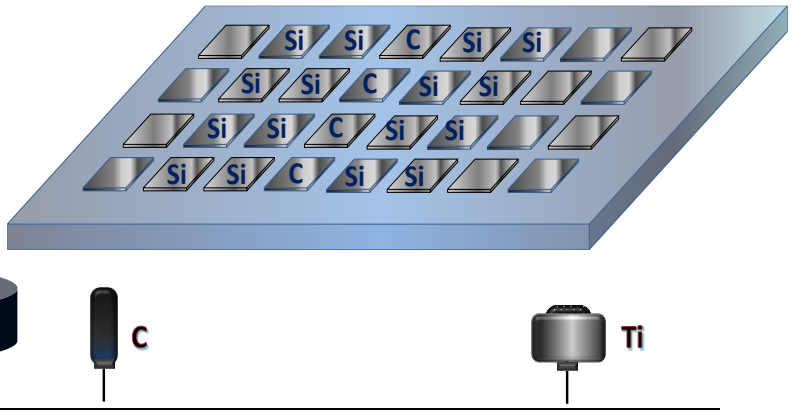


**Figure 3.** Substrates position in holder.

Different batches of samples were obtained by varying the temperature of the substrates and ions acceleration voltage (bias voltage) applied on the sample.

The thickness and the distribution of C and Ti in a layer were highkighted in Table 1. The difference of the various ***B*** samples is due to relative position of the substrates fixed in the holder with respect to the two plasma sources of C and Ti (Fig. 3.). Also, discharge parameters for C and Ti plasmas are highlighted in Table 2 and Table 3 respectively. Here are presented: anode potential $U_a$, discharge current $I_a$, filament current $I_f$, thickness of layer and deposition time. Films deposition rates (0.14nm/s for carbon and 0.18nm/s for Ti) and thickness were in situ monitored using micro-quartz balances (QMB).

**Table 1.** C/Ti layer distribution

| Titanium | Thickness(nm) | Carbon | Thickness(nm) |
|---|---|---|---|
| - | - | 100% | 20.00 |
| 1% | 1.00 | 99% | 39.00 |
| 3% | 2.30 | 97% | 37.70 |
| 5% | 4.00 | 95% | 36.00 |
| 7% | 5.00 | 93% | 35.00 |
| 10% | 7.00 | 90% | 33.00 |
| 15% | 10.00 | 85% | 30.00 |
| 25% | 16.00 | 75% | 24.00 |

**Table 2**. Discharge parameter for C

| No. | $U_a$ (kV) | $I_a$ (A) | $I_f$ (A) | Rate (nm/s) | Thickness (nm) | Time (min) |
|---|---|---|---|---|---|---|
| 1 | 1.86 | 1.14 | 60.80 | 0.01 | 20.0 | 16 |
| 2 | 1.88 | 1.35 | 60.90 | 0.06 | 39.0 | 12 |
| 3 | 1.88 | 1.35 | 60.90 | 0.07 | 37.7 | 8 |
| 4 | 1.89 | 1.34 | 60.90 | 0.07 | 36.0 | 8 |
| 5 | 1.87 | 1.34 | 61.70 | 0.07 | 35.0 | 7 |
| 6 | 1.88 | 1.34 | 61.70 | 0.70 | 33.0 | 7 |
| 7 | 1.90 | 1.34 | 61.70 | 0.80 | 30.0 | 7 |
| 8 | 1.79 | 1.35 | 60.90 | 0.80 | 24.0 | 7 |

**Table 3**. Discharge parameters for Ti

| No. | $U_a$ (kV) | $I_a$ (A) | $I_f$ (A) | Thickness (nm) | Time (min) |
|---|---|---|---|---|---|
| 1 | 1.20 | 0.70 | 50.60 | 1.0 | 12.0 |
| 2 | 1.20 | 0.70 | 50.00 | 2.3 | 8.0 |
| 3 | 1.20 | 0.70 | 49.80 | 4.0 | 8.0 |
| 4 | 1.18 | 0.70 | 50.00 | 5.0 | 7.0 |
| 5 | 1.17 | 0.77 | 49.80 | 7.0 | 7.0 |
| 6 | 1.10 | 0.79 | 47.80 | 10.0 | 7.0 |
| 7 | 1.00 | 0.65 | 44.50 | 16.0 | 7.0 |

## 3. Results and disscusions

### *3.1. RBS measurements*

For providing reliabe quantitative information regarding the composition and the elemental depth profile, Rutherford Backscattering Spectrometry (RBS) measurements were performed on the sample ***B1*** (substrate temperature was room temperature, and bias voltage was 0V). For this purpose the 3MV Tandem Accelerator was used. The sample was mounted on a 3-axes goniometer with an accuracy of 0.01°. Slits were employed to limit the fascicle divergence to a minimum. The Silicon solid-state detector with an energy resolution of 20keV for He particles was positioned at an angle $\theta = 165°$ in respect with the ion beam. The

sample was measured at normal incidence in respect with the beam. A broad beam with dimensions around 0.5mm$^2$ was focused on the samples and mono-energetic He ions with an energy of 3MeV were used to bombard the sample in order to determine the elemental area density and impurity distribution. The different atomic species, areal density, elemental depth profile and the layers thickness were obtained by fitting the simulated spectrum on the experimental one. This was done by using specialized RBS spectrum simulation program SIMRA. Figure 4 and Figure 5 presents the RBS experimental spectra for C-Ti layers and elemental depth profile respectively (sample ***B1***).

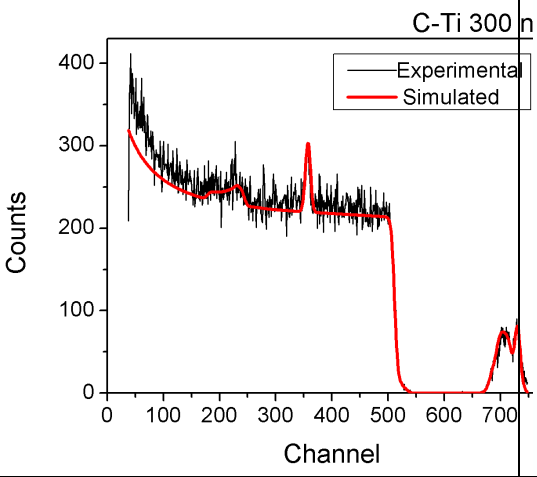


**Figure 4**. Experimental spectrum vs. simulated spectrum

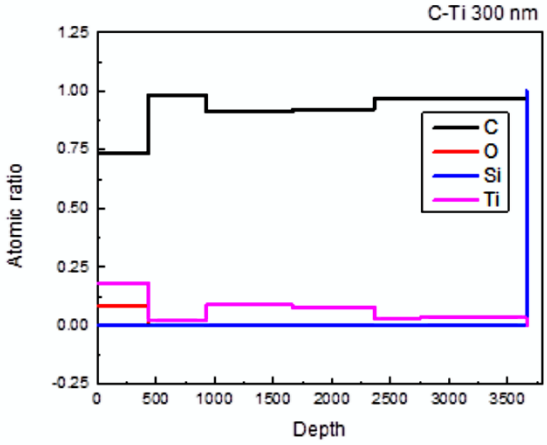


**Figure 5**. Atomic concentration vs. thickness (elemental depth profile)

In order to estimate the areal densities of elements in the film, the spectra was fitted using SIMRA. Figure 4 shows the simulation of the RBS spectra. The simulated (red) and experimental (black) are very well overlapped. There is a very good separation of the film from the substrate due to the excellent resolution of this method for the elements with a large atomic number relative to the silicon (substrate). This is explained by the different loss of proton energy when interacting with Ti or C in comparison with the silicon (substrate). Overlap of Ti and C signals is most likely caused by the films composite structure and the loss of proton energy by binary collisions with the Ti and C nucleus.

The results reveals a homogeneous concentration of carbon and titanium in the sample (Fig. 4). The film does not contain metallic impurities, the inevitable contamination since exposure to atmospheric air, only the Oxygen is found in

these profiles, suggesting a very low concentration of gaseous inclusions below the detector limit. Figure 5 shows also the distribution of C and Ti in the sample; the Ti average concentration is 17% and for C average concentration is 85%. The results obtained were very close to the desired concentration.

### *3.2. Raman measurements*

Figures 6 and 7 highlight Raman spectra in case of 4 samples (***A1*** – deposition: room temperature, bias voltage: 0V; ***A2*** - deposition: room temperature, bias voltage: -700V; ***A3*** - deposition: 300°C, bias voltage: 0V; ***A4*** - deposition: 300°C, bias voltage: -700V; )

The meaurements reveal that peaks apear at around 250, 340, 420, 610, 740, 1340 and 1530-1567cm$^{-1}$, suggesting mixtures of TiC, $Ti_3C_2O_2$ and $Ti_3C_2$ and at 1340, 1560cm$^{-1}$, the characteristic D an G peaks of disordered carbon. The characterstic peaks of $Ti_3C_2O_2$ and $Ti_3C_2$ have vibrational modes at 347, 730 and 621cm$^{-1}$ respectively, peaks at 260 and 420cm$^{-1}$ correspond to TiC. The single crystalline Si-substrate signals appear (c-Si) at around 550 and 1000cm$^{-1}$. The shift shown in the spectra of our samples may occur owing to the mechanical stress.

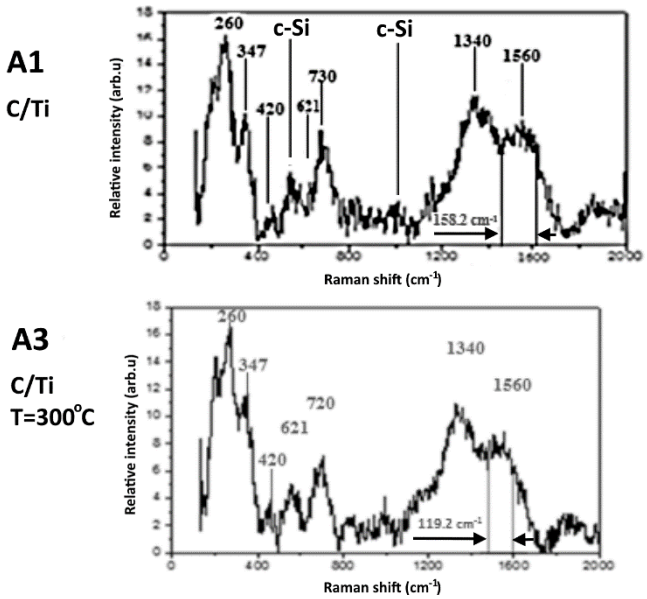


**Figure 6**. Raman spectra in case of ***A1*** (deposition: room temperature, bias voltage: 0V); ***A3*** (deposition: 300°C, bias voltage: 0V);

Following deconvolution of spectra and fitting with a Gauss function, the peaks values were assigned regarding the carbon. In the table 4 are displayed the D and G peaks positions, $I_D$ and $I_G$ values and the corresponding $I_D/I_G$ ratios of the nonreacted carbon in the case of samples A1, A2, A3, A4. The substrate temperature has been at room temperature and at 300°C. This rather low deposition temperature could allow for small amounts of carbon create Ti-C bonding, whereas the unreacted carbon created a film on top of the structure thus explaining the presence of the D and G peks of disordered graphite in the Raman spectrum. The positions of D- and G-peaks and their intensity ratio $I_D/I_G$ provide structural information of the materials. Existance of both peaks in visible Raman spectra is directly related to the ordering of $sp^2$ sites and only indirectly on the fraction of $sp^3$ sites.

The increase of the temperature from room temperature to 300°C determine the decrease of G linewidth in the cases of samples ***A1*** and ***A3*** from about 158.9cm$^{-1}$ to about 119.2cm$^{-1}$ (Fig.6.) and in the cases of samples A2 and A4 from about 172.2cm$^{-1}$ to about 106cm$^{-1}$ (Fig. 7.). Suitable the ratio $I_D/I_G$ increase from 1.009 (sample ***A1***) to 1.450 (sample ***A3***) and from 1.100 (sample ***A2***) to 1.220 (sample ***A4***).

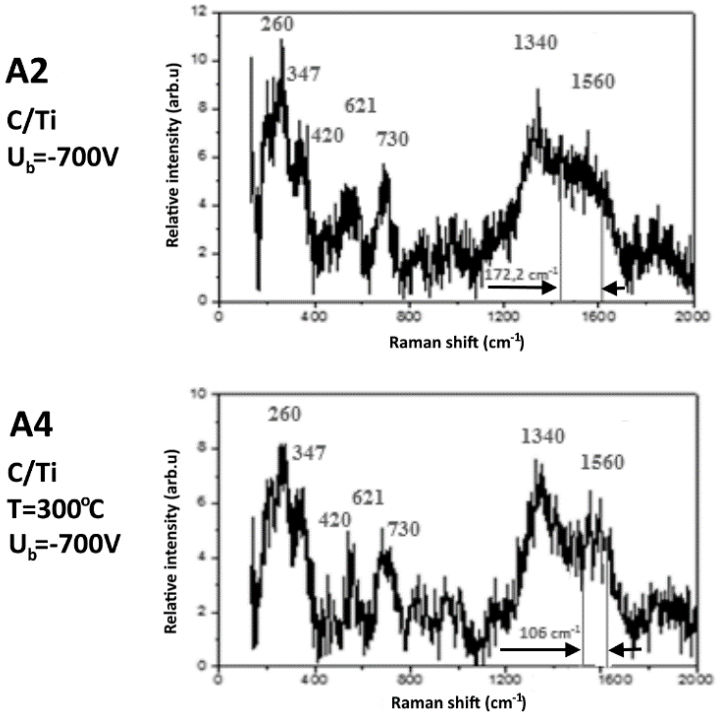

**Figure 7**. Raman spectra in case of ***A2*** (deposition: room temperature, bias voltage: -700V); ***A4*** (deposition: 300°C, bias voltage: -700V);

**Table 4.** Peaks values regarding the carbon for samples ***A1***,***A2***,***A3***,***A4***

| Sample | D[cm$^{-1}$] | G[cm$^{-1}$] | $I_D$ | $I_G$ | $I_D/I_G$ |
|---|---|---|---|---|---|
| A1 | 1337 | 1527 | 671 | 665 | 1.009 |
| A2 | 1344 | 1566 | 995 | 890 | 1.100 |
| A3 | 1336 | 1555 | 2203 | 1501 | 1.450 |
| A4 | 1343 | 1561 | 2148 | 1756 | 1.220 |

According to reference [29] in the case of graphite crystallites $\frac{I_D}{I_G} = \frac{1}{L_a}$ ($L_a$ being graphite crystallite size), the increase of $\frac{I_D}{I_G}$, is determined by decrease of graphite crystallite sizes. In this respect, according to Fig. 8 (HRTEM ***A2***) $L_a \approx 35.5$Å whereas according to Fig. 9 (HRTEM ***A4***) $L_a \approx 21.5$Å. We mention the fact that according to reference [3] the decrease of graphite crystallite sizes as result of increase of the deposition temperature is correlated with increase of TiC crystallite size with increase of deposition temperature. We consider that the decrease of ratio $\frac{I_D}{I_G}$ from 1.450 in the case of sample ***A3*** to 1.220 in the case of sample ***A4*** is due to increase of crystallite sizes caused by -700V bias potential applied on the sample ***A4***

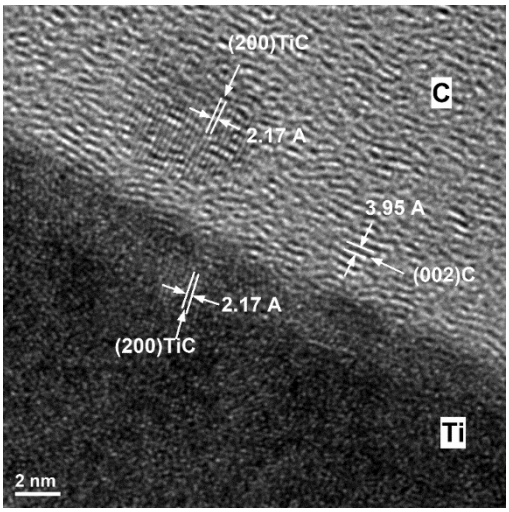


**Figure 8**. HRTEM image of sample ***A2***

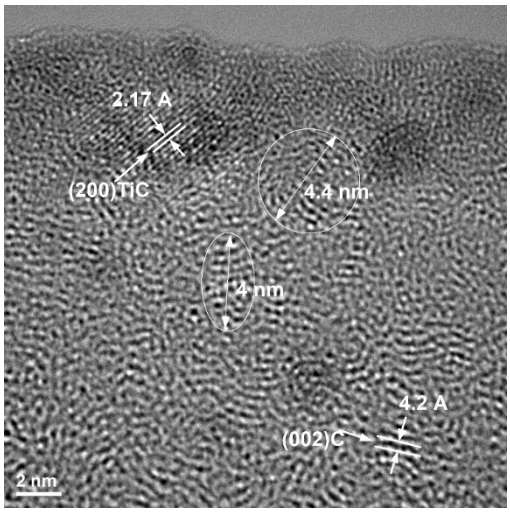


**Figure 9**. HRTEM image of sample ***A4***

### *3.3. TEM measurements*

The characterization of microstructure properties of as prepared C-Ti multilayer structures were done using Electron Microscopy techniques (TEM). The microstructure properties was studies using transmission electron microscope CM120 and Philips Tecnai F30G2 at 300kV set-up.

Analysis of diffraction patterns was perfomed using CRISP2 application, with the crystalline material module (ELD). The indenxing of lines extracted from the profile was done by comparative method.

In Figs. 10, 11 and 12 respectively, are presented the extracted profiles from diffraction patterns in the case of samples ***A1***, ***A3*** and ***A4*** respectively. These figures contain also the appropriate granular structures of samples.

Fig. 10 show that sample ***A1*** is a granular film to amorphous with very small crystal size, with a very wide peak at 0.240nm. We can also identify two adjacent, less intense peaks at 0.260nm and 0.218nm respectively, followed by a wide peak at 0.152nm, and other peaks at 0.126nm, 0.117nm and 0.095nm. These values can be associated with the cubic TiC structure[30].

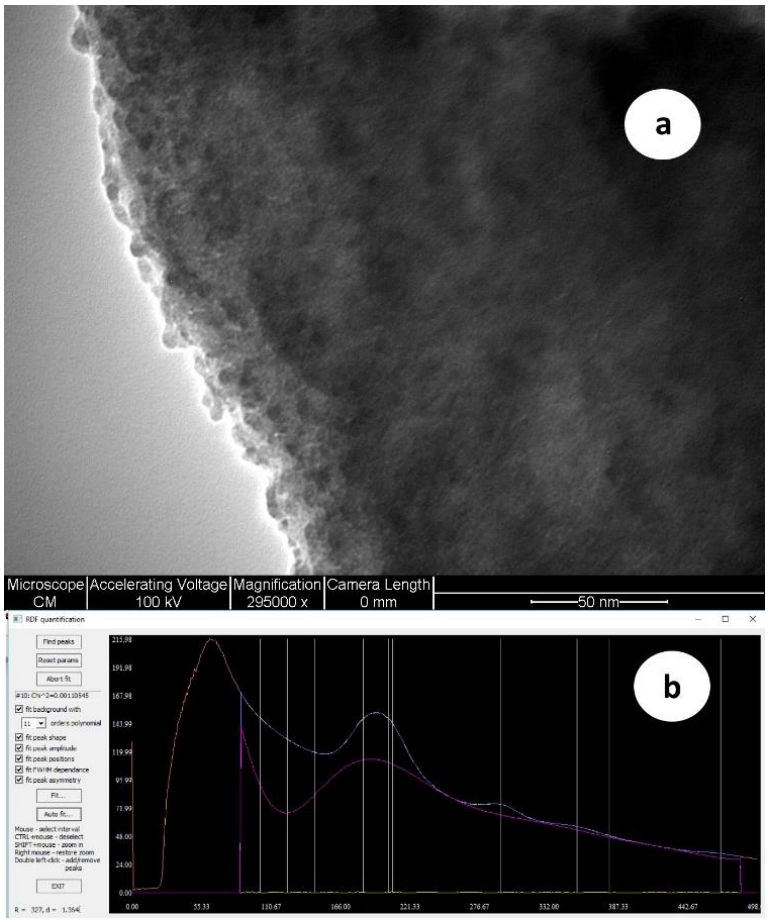


**Figure 10**. (a) Granular structure of multilayer film from sample ***A1***.
(b) Extracted profile from diffraction pattern

The extracted profile presented in Fig.11b reveal the fact that sample ***A3*** shows the presence of a granular film with very small crystal size, with a very wide peak at 0.232nm. Two less intense additions are also identified at 0.260mn and 0.210nm, respectively. (Fig.11b). These values can be related to the TiC cubic structure. The other values identified in the profile are very low and do not have enough credibility to be taken into account for phase identification.

In the case of sample ***A4*** results from the extracted profile (Fig. 12b) show that the structure of the film is crystalline, with peaks identified at characteristic values of a cubic TiC film. Also, the electron diffraction shows that the film presents another phase with peak of 0.321nm which can be attributed to titanium oxide with tetragonal structure (rutile). Peaks from 0.377nm and 0.277nm have been added to minimize errors during profile fitting.

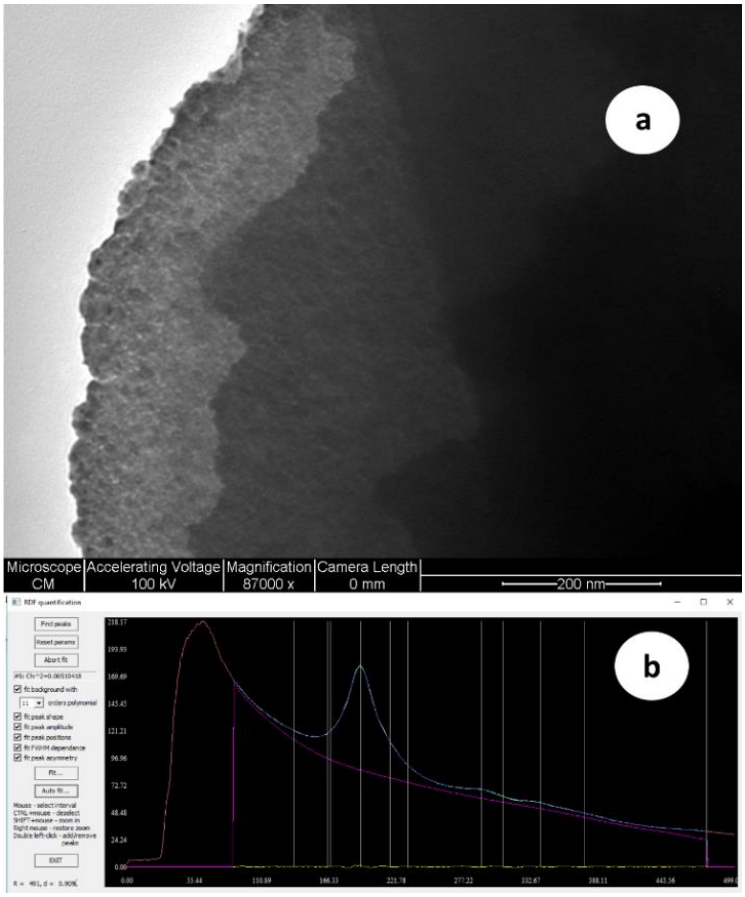


**Figure 11.** (a) Granular structure of multilayer film from sample ***A3***.
(b) Extracted profile from diffraction pattern

In Fig. 13 is presented the extracted profile from diffraction pattern for sample ***B1***. (cabon-titanium film having the structure as in Table 1). Here is presented also the appropriate polycrystalline structure area from sample. Electron diffraction shows the presence of a polycrystalline film with diffraction peaks values of 0.249nm, 0.214nm, 0.151nm, 0.129nm, 0.123nm; these values are characteristic of a TiC cubic structure[30].

Another group of samples used for measurements were ***A5*** (temperature of substrate was room temperature; the thickness of Ti layers was 20nm); ***A6*** (temperature of substrate was room temperature; the thickness of Ti layers was 16nm); ***A7*** (temperature of substrate was 300ºC; the thickness of Ti layers was 20nm); ***A8*** (temperature of substrate was 300ºC; the thickness of Ti layers was 16nm). Figure 14 shows a stripped area of the deposited film from sample ***A5***.

The diffraction pattern in the area selected for investigation confirms the presence of a granular material, crystallized. The profile drawn from the diffraction pattern is shown in Fig. 14b, respectively.

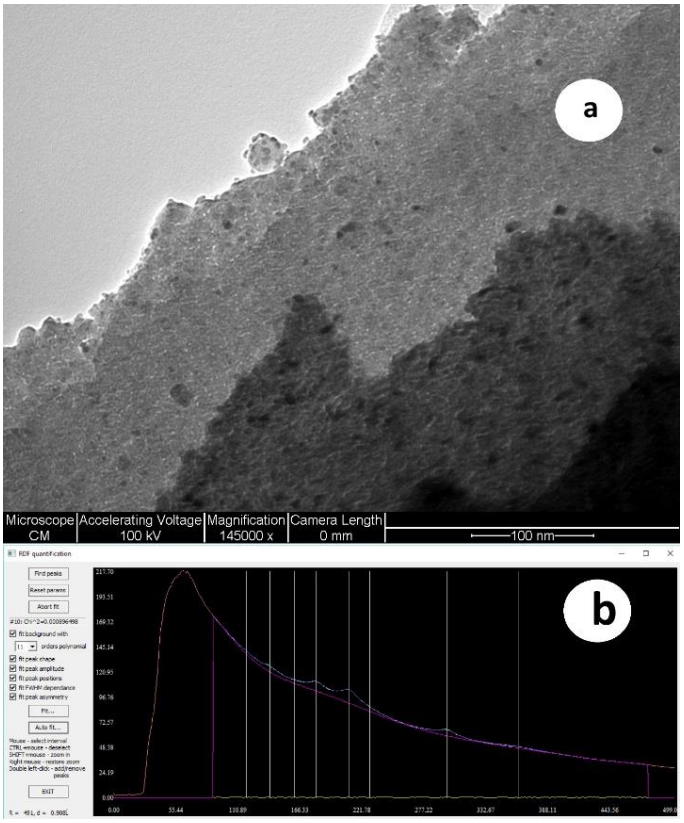


**Figure 12**. (a) Granular structure of multilayer film from sample ***A4***. (b) Extracted profile from diffraction pattern

From the comparision of values with the lines identified for Ti and TiC, the peaks detected were indexed. The size of the crystalline area determined by Scherrer method is 5.25nm. We see large errors in the use of the Cohen method for the cubic structure of TiC. For the cubic structure of TiC we have 2.13%, for parameter ***a***, and 0.26% and 0.67% for the parameters ***a*** and ***c*** respectively, in the case of the hexagonal structure of Ti. Thus, we can choose the phase for this sample, Ti, with hexagonal structure. The Williamson-Hull curve confirms these errors, resulting in a relative deformation of the network $\varepsilon = + 0.0025$.

The area selected for analysis from sample ***A6*** and the profile drawn from the diffraction pattern are shown in Figure 15. From the comparison of the values

with the lines identified for Ti respectively TiC, we can associate the cubic structure with faces centered on this sample (TiC).

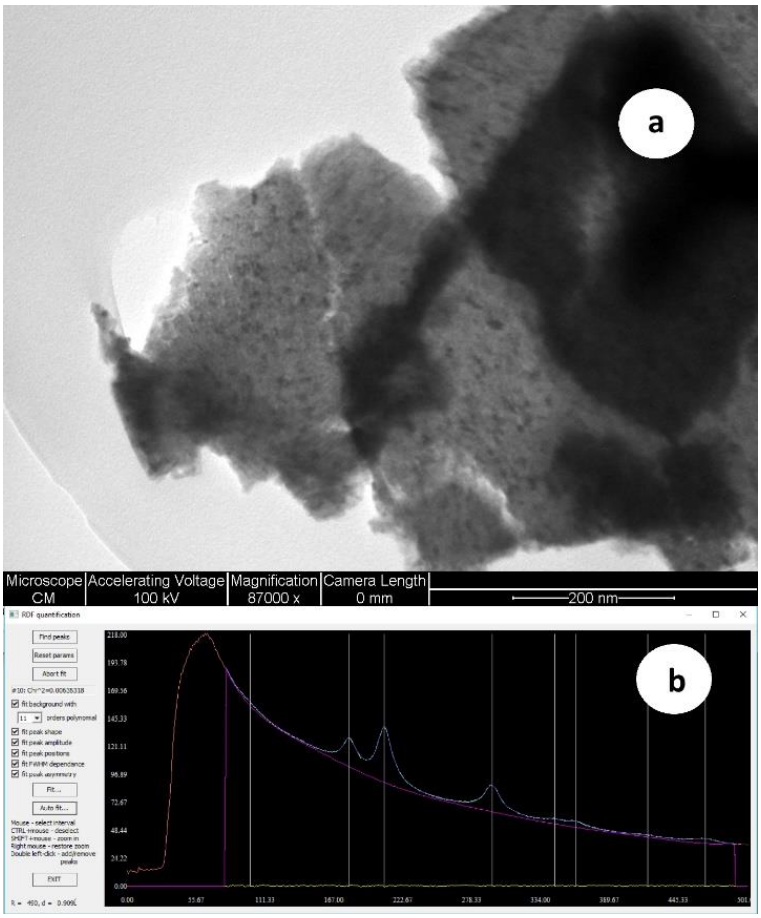


**Figure 13.** (a) Polycrystallinic film area from sample ***B1*** ,
(b) Extracted profile from diffraction figure

Errors for validating the hexagonal structure of Ti are much greater. The size of the crystalline area determined by Scherrer methods is 2.3nm.

There are some major errors in using the Cohen method. The error of -21.07% for parameter ***c*** of the hexagonal structure indicates that the most probable structure is cubic (errors for parameter ***a***, 4.64%). The Williamson-Hall curve confirms these errors, resulting in a relative deformation of the network $\varepsilon = -0.011$

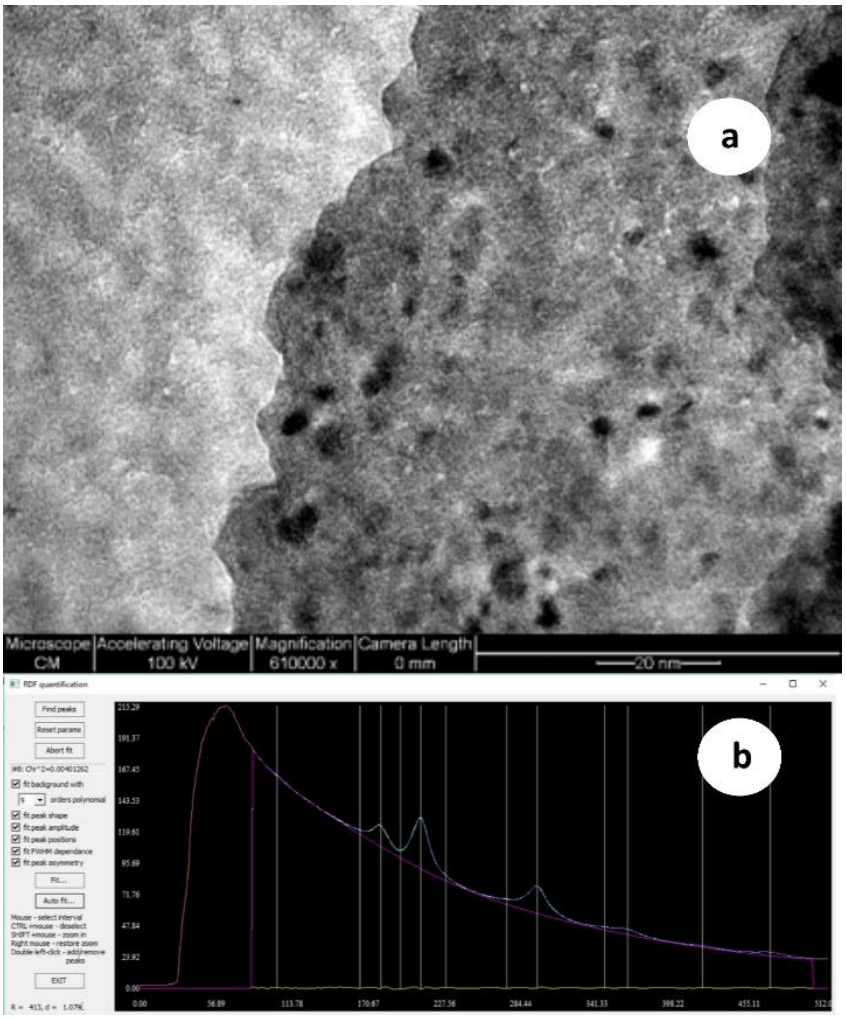


**Figure 14**. (a) Granular structure of multilayer film from sample ***A5*** ,
(b) Extracted profile from diffraction figure

.

The Fig. 16 shows the area selected for investigation from sample ***A7*** and the extracted profile from the diffraction pattern. Using the procedure presented above, were obtained the errors: for the cubic structure of TiC -0.322%, respectively 2.28% and 1.23% for the hexagonal structure of Ti. The size of the crystalline area determined by Scherrer methods is 4.038nm. For this sample, we can say that we have a mixture of phases, cubic TiC and hexagonal Ti. The Williamson-Hull curve confirms these errors, resulting in a relative deformation of the lattice $\varepsilon = -0.00324$.

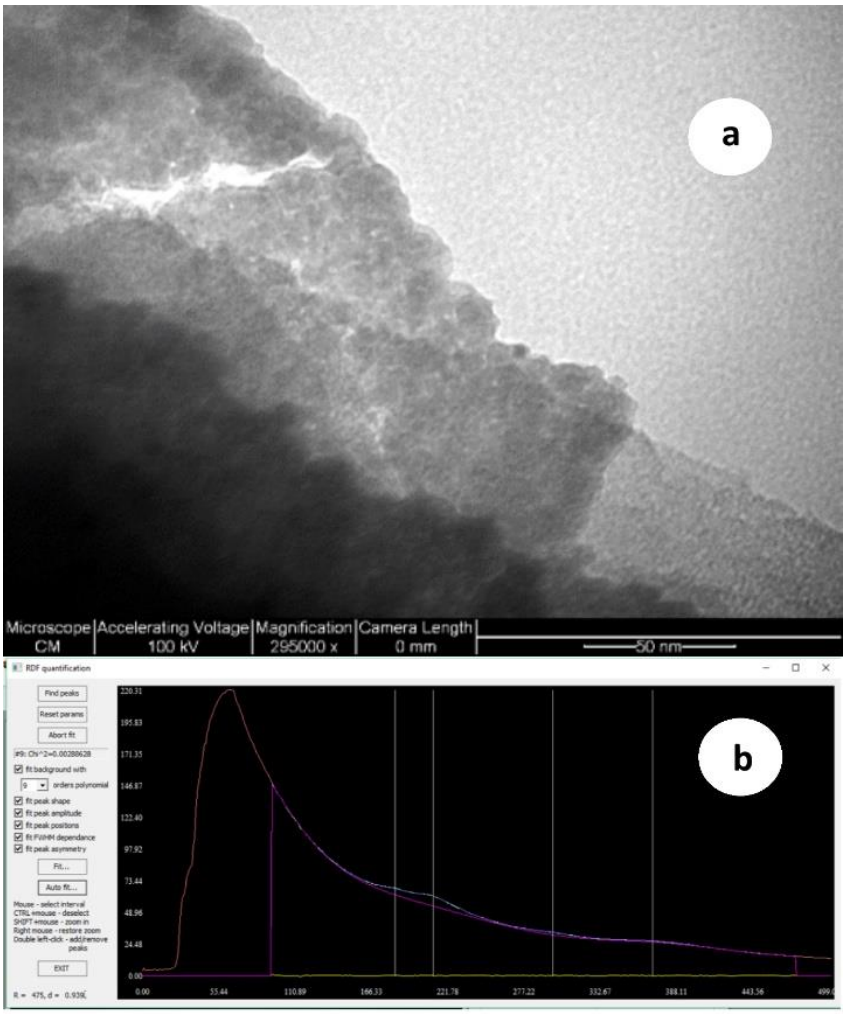


**Figure 15.** (a) Granular structure of multilayer film from sample ***A6*** ,
(b) Extracted profile from diffraction figure

The Fig. 17a reveals a granular area selected for analysis from sample **A8**. The diffraction pattern in the area selected confirms the presence of a granular material, crystallized. The profile drawn from the diffraction pattern is shown in Fig. 17b. From the comparison of the values with the lines identified for Ti, respectively TiC, we can associate the cubic structure with faces centered on this sample.

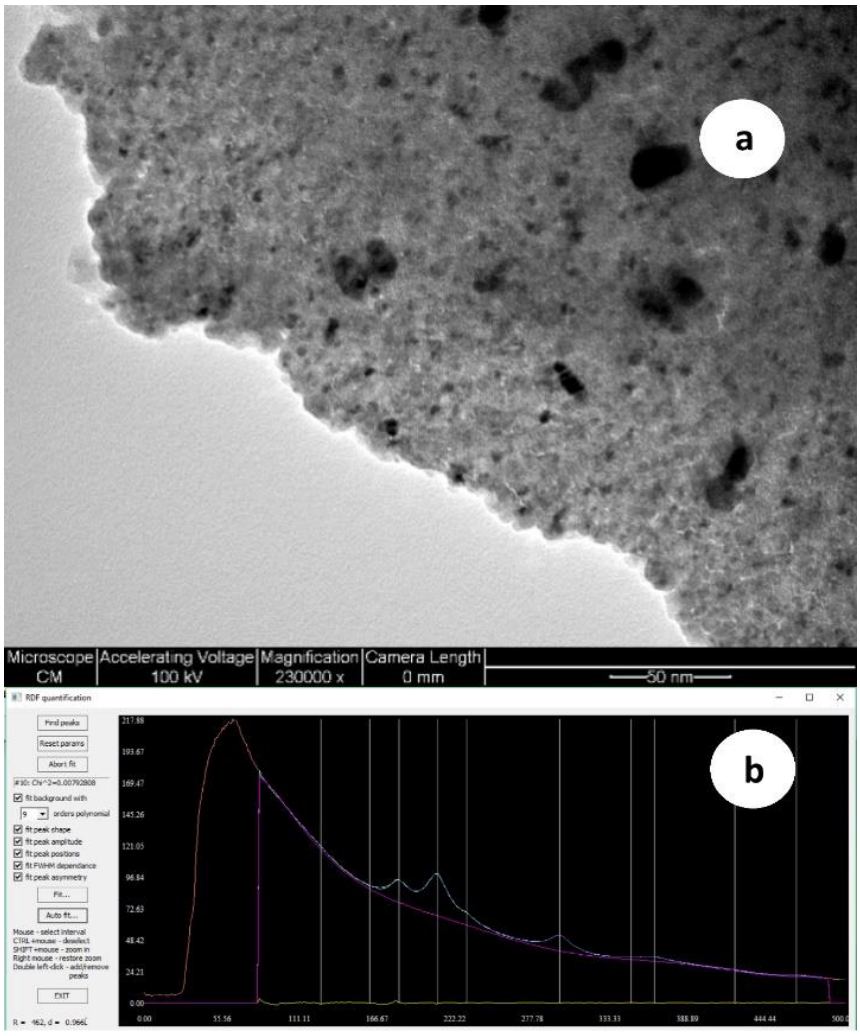


**Figure 16.** (a) Granular structure of multilayer film from sample ***A7*** , (b) Extracted profile from diffraction figure (Sample ***A7***)

Errors for validating the hexagonal structure of Ti are much greater. The size of the crystalline area is 6.69nm. There are some major errors in using the Cohen method. For the cubic structure of TiC we have 3.18%, and -2.30% and -3.95% respectively for the hexagonal structure of Ti. In this sample the errors are comparable, so there is the possibility of a mixture of phases, Ti + TiC. The Williamson-Hull curve confirms these errors, resulting in a relative deformation of the network $\varepsilon = -0.0055$.

It can be observed that in the case of samples ***A5*** and ***A7*** with the same thickness of Ti layers (20nm) the increaase of the substrate temperature from room temperature (sample ***A5***) to 300°C (sample ***A7***) causes a passage from predominant hexagonal Ti phase (sample ***A5***) to a cubic TiC and hexagonal Ti mixture of phases (sample ***A7***) This observation is in agreement with reference [6] were is studied the effect of synthesis condition on the formation of the TiC phase on Si substrate by DC magnetron ion-plasma sputtering of combined graphite/titanium target. The authors show that increase of temperature allows to synthesized films with stoichiometry that coincid with that of TiC.

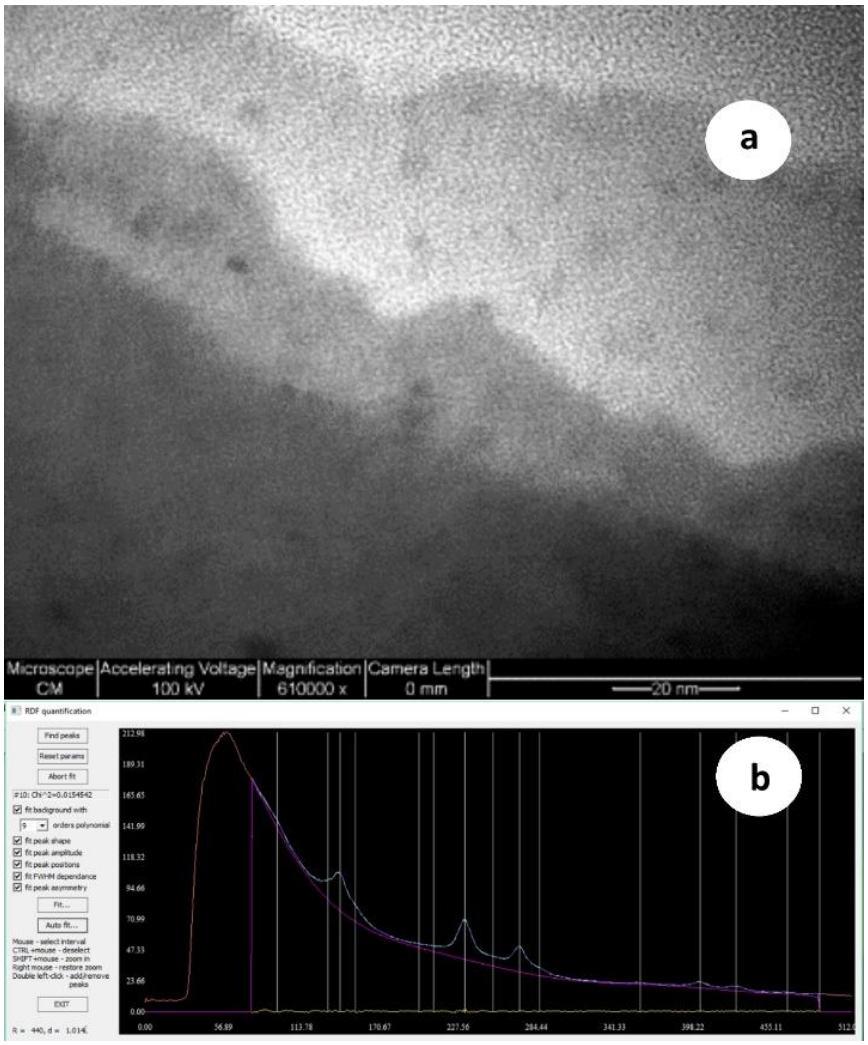


**Figure 17.** (a) Granular structure of multilayer film from sample ***A8*** , (b) Extracted profile from diffraction figure (Sample ***A8***)

In the case of sample ***A6*** and ***A8*** with the thickness of 16nm Ti layers, the predominance of cubic TiC phase in both cases can be explained by intensifying the diffusion processes at Ti/C interfaces, in comparision with samples ***A5*** and ***A7***, as a result of the decrease of the thickness of Ti layers at 16nm.

This ascertainment is consistent with reference [8]. The authors of study [8] present titanium/diamond-like carbon bilayer films with different relative thickness fabricated by direct-current and pulsed cathode arc plasma method, showing the microstructure evolution (the size and ordering degree of $sp^2$-hybridized carbon clusters) with varying the thickness of Ti interlayer. Nano-scales Ti interlayer of 12-20nm thickness presents the largest size effect. The catalytic effect of the sublayer is most pronounced in the carbon layer of less than 106 nm. In these thickness ranges, ractivity between atoms at intereface is highest. These results are asociated with the occurrence of atomic diffusion process at Ti/C interface.

Considerations to formation of TiC and Ti phases was also made in reference [7]. In this case, thin layers were deposited by DC magnetron sputtering at room temperature from Ti and C targets. Cubic TiC was formed from ***A8*** to 86at.%Ti.

HRTEM was used both morphological and structural features of multilayer structure using Philips Tecnai F30G2 at 300kV set-up. To obtain the detail features of multilayer structures was used XTEM sample preparation, final thickness being obtained using Fischione IonMill model 1010. To eliminate all milling residue from the sample a plasma cleaner was used. The geometry of the samples ***A2*** and sample ***B2*** ( structure as in Table 1, deposition temperature: room temperature, bias voltage: 0V ) are presented in Fig. 18 and Fig. 19 respectively.

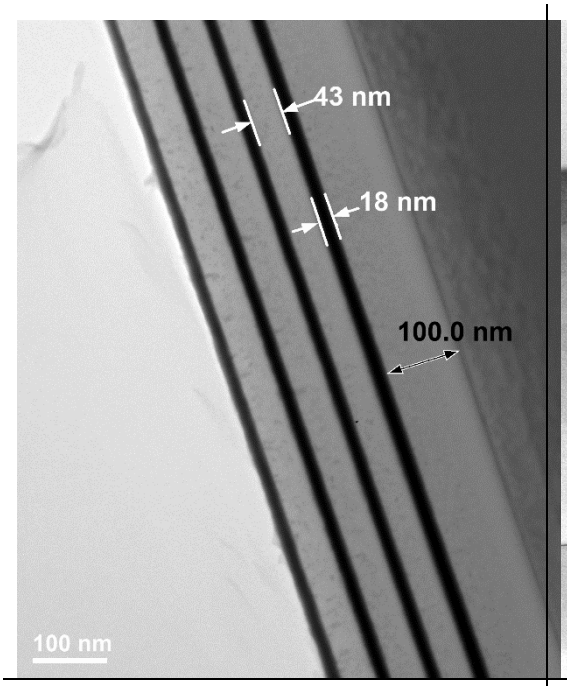


**Figure 18**. The geometry of sample ***A2*** at scale 100nm.

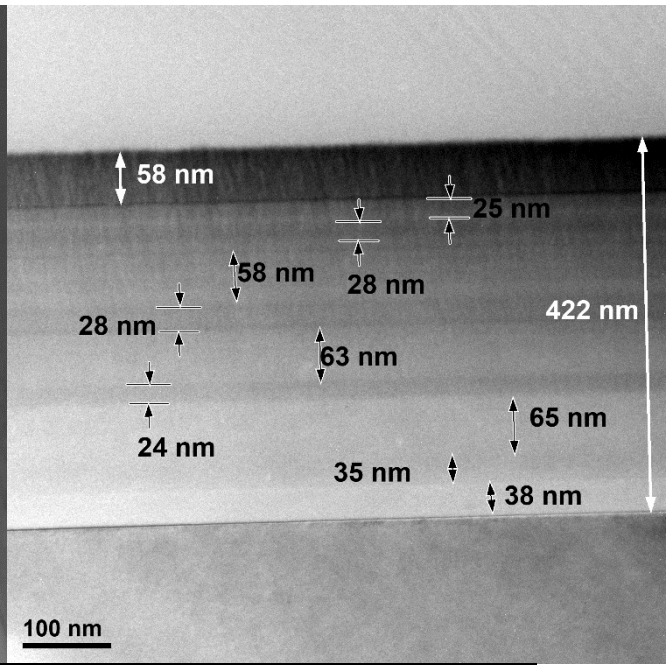


**Figure 19**. The geometry of sample **B2** at scale 100nm.

To perform EDX spectra in different position within the examinated structures, they were chosen the areas edx1; edx2; … as can see in Fig. 20 for sample ***A4*** and Fig. 21 for sample ***B2***; in the case of sample B2 the areas A,B, … correspond to the areas worked in Fig. 19.

In Fig. 22 is displayed a HRTEM image performed in the area edx5 from sample ***A1***, in accordance with Fig. 20. Crystallized areas with sizes of 2.5nm, 3.9nm and 5.3nm in amorphous carbon are observed. These crystallites can be mixtures of TiC, $Ti_3C_2O_2$ and $Ti_3C_2$ confirming Raman measurements (Fig.6). Fig. 23 highlights the HRTEM image at interface 1 between Si support layer and Carbon base layer A from sample ***B1*** (see Fig. 21). In Fig. 24 is presented a HRTEM image with FFT performed in area I (from Fig.21) in the case of sample ***B1***; the measurments reveal the presence of the TiC cubic phaseThe measurments reveal also that degree of crystallization increase from area A to area I.

EDX spectra for sample B1 are presented in Fig. 25; from here we can obtain the percentages for C and for Ti in the areas of interest as follows: edx2(97.14%C, 2.86%Ti), edx3(99.49%C, 0.51%Ti), edx4(88.64%C, 11.36%Ti), edx5(90.57%C, 9.43%Ti), edx6(83.33%C, 16.67%Ti), edx7(81.54%C, 18.46%Ti), edx8(73.85%C, 26.15%Ti), edx9(72.88%C, 27.12%Ti), edx10(66.67%C,

33.33%Ti), edx11(65.12%C, 34.88%Ti), edx12(90.23%C, 9.77%Ti). The presence of elements W and Fe may be attributed to undesirable residues in the deposition chamber.

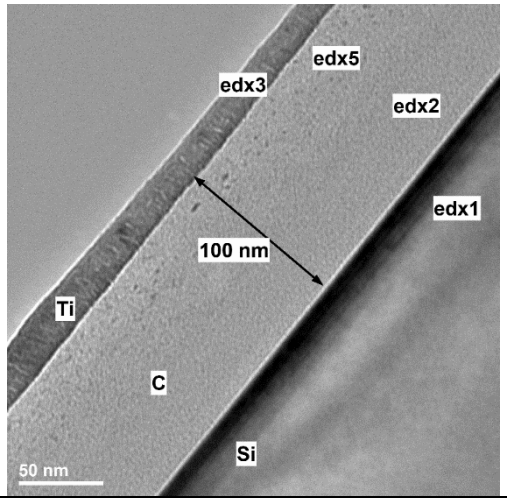


**Figure 20.** The areas for EDX studies in the case of sample *A4*

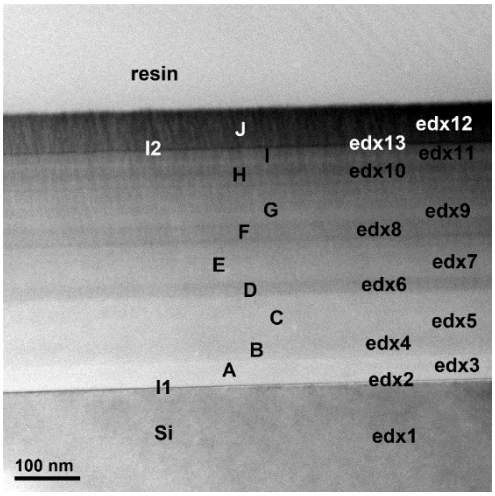


**Figure 21**. The areas for EDX studies in the case of sample ***B2***

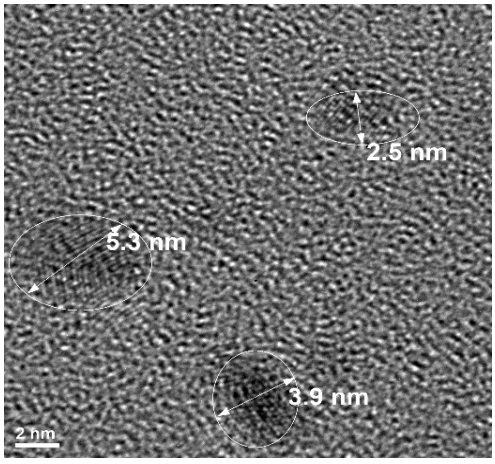


**Figure 22**. Crystallized areas with sizes of 2.5nm, 3.9nm and 5.3nm in amorphous carbon (sample ***A1***)

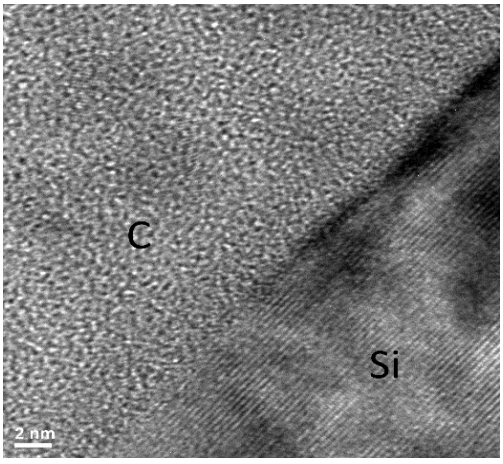


**Figure 23**. HRTEM image of interface between Si support and C base layer (Sample ***B1***)

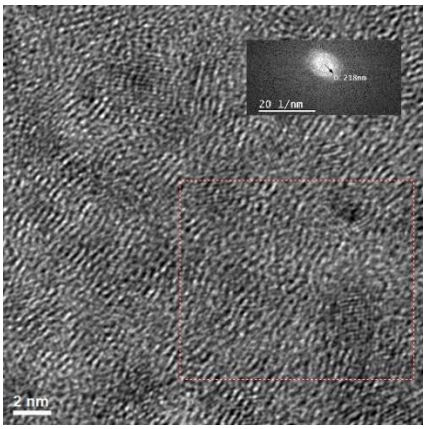


**Figure 24**. HRTEM image which reveal TiC cubic phase (Sample ***B1***)

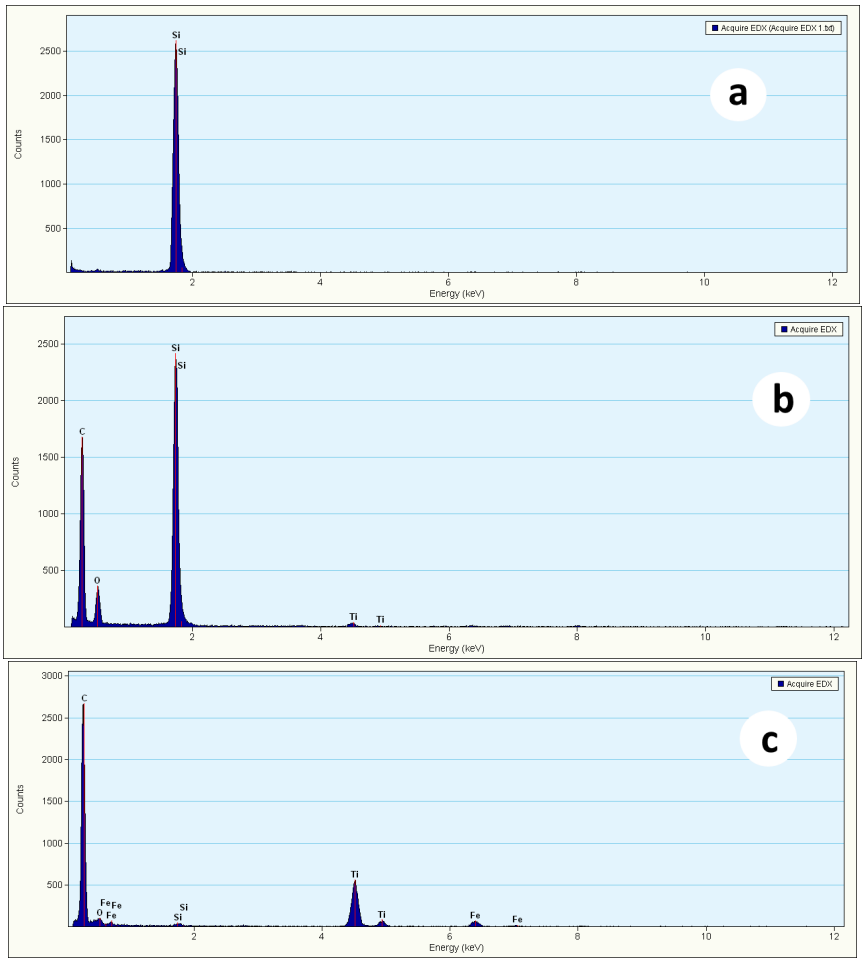

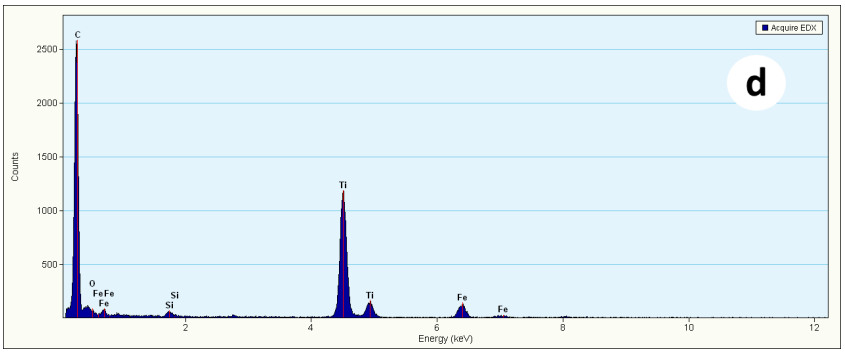


**Figure 25.** EDX spectra for sample B1 in the areas of interest in accordance with Fig. 21; (a) EDX1, (B) EDX2, (C) EDX7 AND (D) EDX10

### *3.4. Grazing Incidence X-ray Diffraction (GIXRD)*

The structural investigation of the C-Ti thin films is performed by Grazing Incidence X-ray diffraction (GIXRD) using a Rigaku SmartLab diffractometer provided with Cu Kα radiation (λ = 1.54178 Å), cross-beam optics (CBO) and high energy resolution 2D Hybrid Pixel Array Detector (HPAD) HyPix-3000 in 0D mode. The incidence angles were optimized to the thickness of each sample, taking values between 0.28° ÷ 0.60°.

In the case of multilayers samples the crystalline phases for samples $A_1$(25°C substrate deposition temperature), $A_2$(100°C), $A_3$(200°C), $A_4$(300°C), $A_5$(300°C, -700V bias voltage) and $A_6$(400°C) are show in Fig. 26. The c-TiC phase (TiC, face-centered cubic lattice, space group Fm-3m (225), PDF 04-004-2919) is present as a majority phase in the sample $A_2$(deposited at 100°C). The mean crystallites size for (200) is 6.6 nm.

The sample $A_3$ is 50% amorphous and c-TiC is absent In the remaining samples, c-TiC is present as a minority phase in different concentrations (Ti or titanium oxide hexagonal phases are present). In the sample $M_6$ (obtained at 400°C) only face-centered cubic phases can be found. If the deposition parameters will be improved, and oxygen will be removed, only Ti-C face-centered cubic phases will be obtained, meaning that all titanium atoms will react with carbon atoms. It has a thickness of 71nm, according to the X-ray reflectometry (XRR) measurements.

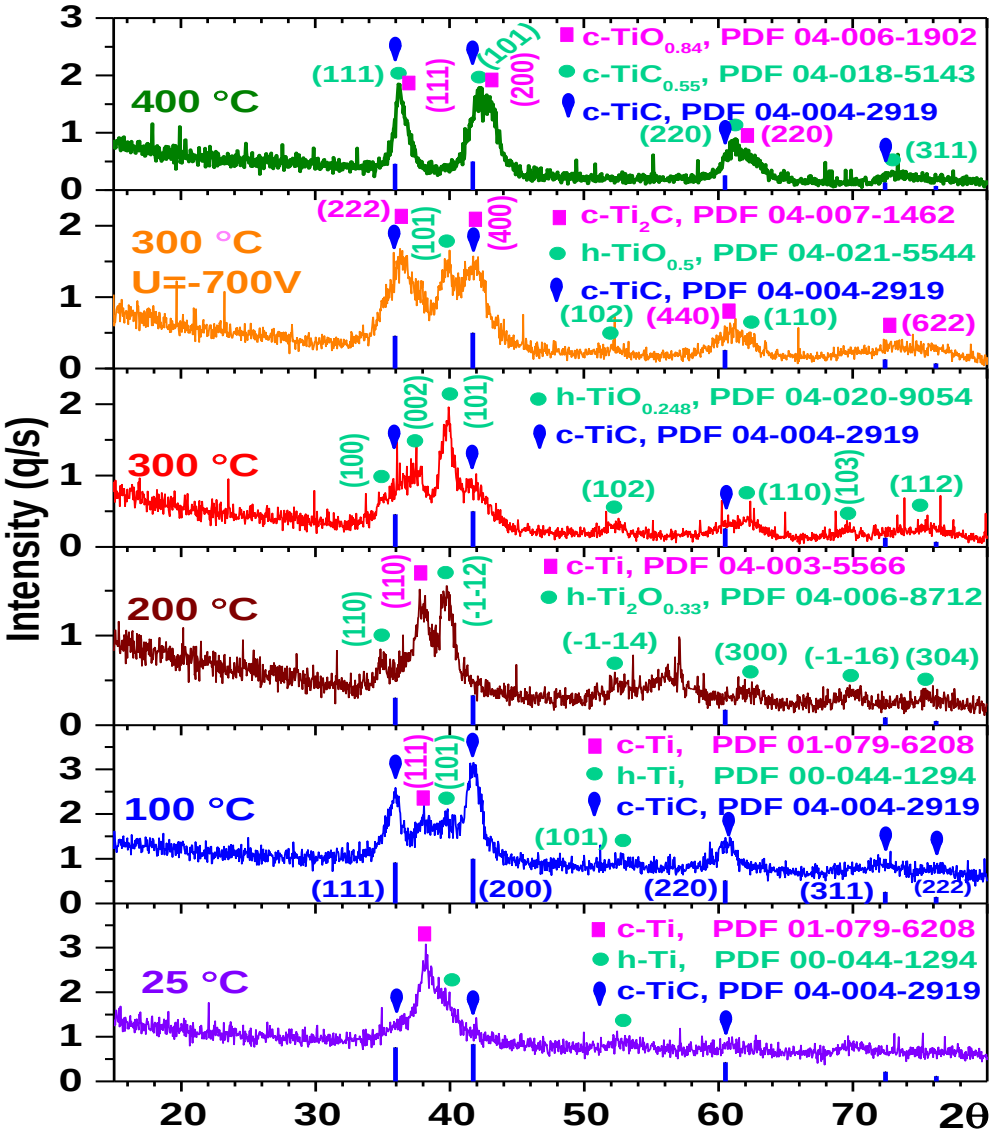


**Figure 26**. X-ray diffraction patterns of the Ti-C thin films deposited at different substrate temperatures: Multilayers samples $A_1$(25°C), $A_2$(100°C), $A_3$(200°C), $A_4$(300°C), $A_5$(300°C, -700V) and $A_6$(400°C).

For codeposition samples the crystalline phases for samples $B_1$(25°C substrate deposition temperature), $B_2$(100°C), $B_3$(200°C), $B_4$(300°C), $B_5$(300°C, -700V bias voltage) and $B_6$(400°C) are show in Fig. 3b. In the sample $B_6$(deposited at400°C) a single polycrystalline phase is found (TiC0.4O0.6, face-centered cubic lattice, space group Fm-3m (225), PDF 04-021-7421).

### *3.5. Tribological measurements*

Tribological measurements were performed using a ball-on-disk tribometer with normal force of 0.5, 1.0, 2.0, 3.0N, respectively. Fig. 26 present the dependence of friction coeficient μ according the distance at different values of normal force, for samples ***A1***, ***A2***, ***A3*** and ***A4***.

The measurements highlighted a decrease of the friction coeficient and breaking distance with the increase of the normal load (for example, in the case of sample ***A3***, at distance 20cm, μ decrease from 0.25 to 0.15 when the load increase from 0.5N to 3N). Analogous situations are also found in the case of samples ***A1***, ***A2*** and ***A4***.

We supposed these results are associated with the occurrence of atomic diffusion processes at Ti/C interface and with appearance of the $Ti_xC_y$ phases.

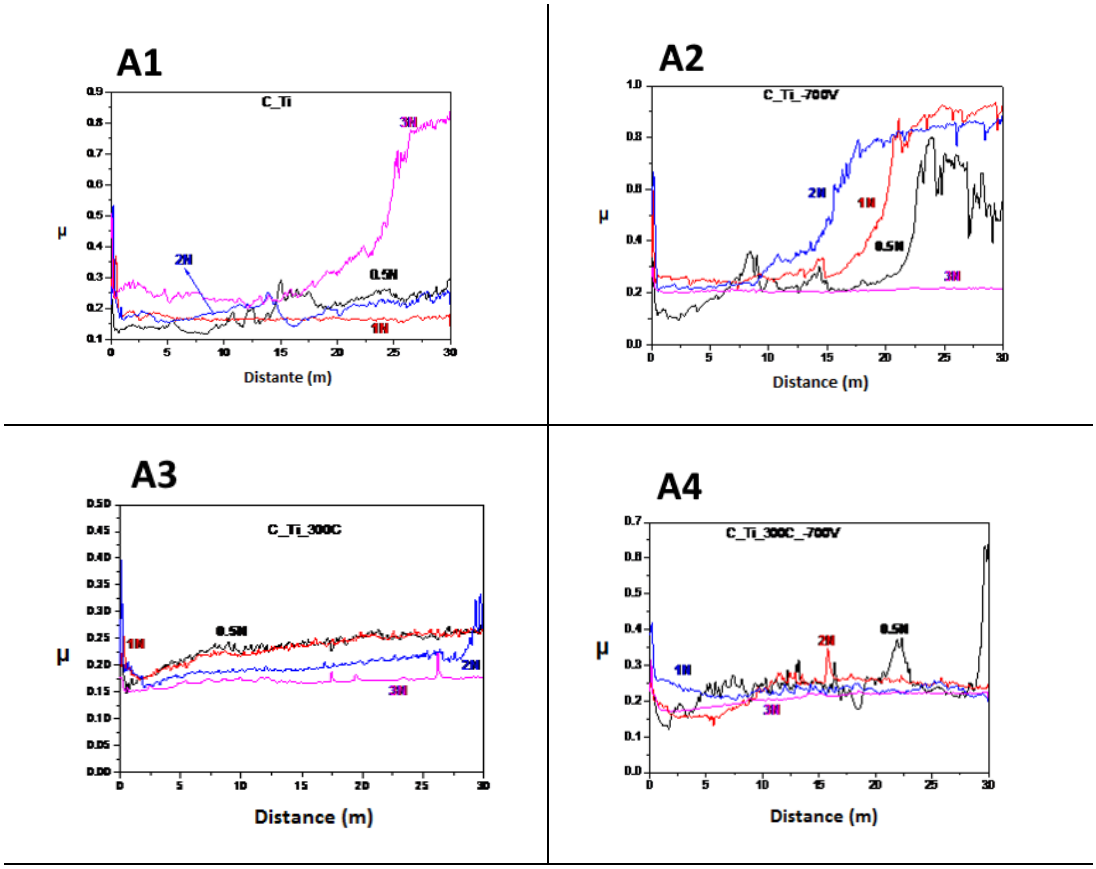


**Figure 27**. Friction coefficient according the distance at normal force of 0.5, 1.0, 2.0, 3.0N for sample ***A1***, ***A2***, ***A3*** and ***A4***.

Based on Fig. 27 we can conclude that an increase of the substrate temperature from room temperature to 300ºC, at a constant value of the bias potential $U_b = -700V$, determines a decrease of the friction coefficient as follows: at normal force of 0.5N and at distance of 20m, from 0.80 (***A2***) to 0.25 (***A4***); at normal force of 1.0N and at distance of 25m, from 0.95 (***A2***) to 0.20 (***A4***); at normal force of 2.0N and at distance of 25m, from 0.85 (***A2***) to 0.19 (***A4***). On the other hand, an increase of the bias potential from 0V to -700V, at room temperature, determines an increase of the friction coefficient as follows: at normal force of 0.5N and at distance of 20m, from 0.2 (***A1***) to 0.8 (***A2***); at normal force of 1.0N and at distance of 25m, from 0.15 (***A1***) to 0.92 (***A2***); at normal force of 2.0N and at distance of 25m, from 0.2 (***A1***) to 0.85 (***A2***). We supposed these results are associated with the occurrences of atomic diffusion process at Ti/C interface and with the appearance of $Ti_xC_y$ phase.

Friction coefficient measurements for titanium and carbon content nanostructures show that the presence of $Ti_xC_y$ phase causes a decrease of the friction coefficient.

Thus, the nanostructures of TiC/a-C:H deposited by unbalanced reactive magnetron sputtering of Ti in an active acetylene containing atmosphere [11] show low friction coefficient. In the case of the Titanium doped diamond-like carbon nanocomposite films with different Ti content obtained by closed field enhanced magnetron sputtering [15], nano-TiC phases and amorphous carbon determine very low friction coefficient. These studies on the Ti doped amorphous carbon multilayers films with different Ti content deposed on medical Ti6Al4V alloy using a closed field enhanced magnetron sputtering technology [13] outlines a significant influence of the Ti content on the tribological properties. Thus, these films displays law friction coefficients. Also, in the case of Ti6Al4Valloy carburized in salt bath [10] at the 300N pressure, the friction coefficient is decreased from 0.34 before carburizing to 0.15 after carburizing, which shows that the appearance of phase carbide $Ti_8C_5$ as results of carburizing process, improves the friction properties of the alloy speciments surface.

On the other hand, the friction coefficient of the alloy speciments carburized surface decrease from 0.28 to 0.15 when the pressure increase from 100N to 300N.

### *3.6. Electrical measurements*

Electrical surface resistance of carbon-titanium multilayer coating on silicon samples was studied on a temperature range above room temperature. The resistance of the sample, was obtained by comparing voltage drop on the sample

with the voltage drop on a standard resistance in constant current mode. Electrical resistivity is calculated from electrical resistance using sample geometry and than electrical conductivity. The ohmic electrical contacts on the samples was performed by a product consiting of 80% silver-filled two-component epoxy-based glue (0.0025Ω·cm specific resistance).

In Tab. 5 and Tab. 6 are given the values of the electrical conductivity σ at different temperatures for sample ***A2*** and for sample ***B1*** respectively.

**Table 5**. Electrical conductivity σ and thermal coductivity K for sample ***A2***

| T(K) | 340 | 350 | 360 | 370 | 380 |
|---|---|---|---|---|---|
| $\sigma\ (\Omega^{-1}\cdot m^{-1})\cdot 10^{3}$ | 2.043 | 1.540 | 1.450 | 1.430 | 1.090 |
| $K(W\cdot m^{-1}\cdot K^{-1})10^{-2}$ | 1.695 | 1.315 | 1.275 | 1.291 | 1.010 |

**Table 6**. Electrical conductivity σ and thermal coductivity K for sample ***B1***

| T(K) | 300 | 310 | 320 | 330 | 335 |
|---|---|---|---|---|---|
| $\sigma\ (\Omega^{-1}\cdot m^{-1})\cdot 10^{3}$ | 8.726 | 8.803 | 8.881 | 8.945 | 8.977 |
| $K(W\cdot m^{-1}\cdot K^{-1})10^{-2}$ | 6.388 | 6.659 | 6.934 | 7.303 | 7.338 |

Using the Widemann-Franz law, which links the thermal conductivity K to the electrical conductivity σ, at a given value of temperature T ($K = L\cdot T\cdot \sigma$ here $L = 2.44\cdot 10^{-8} W\cdot \Omega\cdot K^{-2}$ being the Lorentz number) was calculated the thermal conductivity K (Tab.5 and Tab.6).

Based on data from Tab.5 and Tab.6 we calculated the value of temperature coefficient of the resistance in the case of sample ***A2***, $\alpha = 1.71\cdot 10^{-2} K^{-1}$, and in the case of sample ***B1***, $\alpha = -8.42\cdot 10^{-4} K^{-1}$.

## 4. Conclusions

Carbon-Titanium (C-Ti) multilayer films were deposited on silicon substrates by means of Thermionic Vacuum Arc (TVA) method. The coated layers consisted of a base layer of about 100nm of Carbon and seven Carbon and Titanium layers depositied alternatively, at different substrate temperature values and different substrate bias voltages values.

The film thickness is content in the interval 159.4nm- 462.5nm. In a second way of working, the coated films consist of a about 20nm carbon base layer and

seven 40nm thickness carbon and titanium layers, the thickness of the structures being between 300nm and 433nm.

Quantitative information regarding the composites and the elements depths profile was performed by RBS measurements using the 3MV Tandem Accelerator.

Peaks revealed by RAMAN spectra are observed at around 250, 340, 420, 610, 740, 1340 and 1530-1567cm$^{-1}$, suggesting mixtures of TiC, $Ti_3C_2O_2$ and $Ti_3C_2$ according to unreacted carbon (1340, 1560cm$^{-1}$, the characteristic D and G peaks of disordered carbon).

HRTEM images, confirm the presence of local crystalline organization of TiC in chosen areas based on XTEM sample preparation.The identification of the structure of the material was based also on the data from diffraction pattern using CRISP2 application with the crystalline material module (ELD).

The GIXRD measurements show that the c-TiC phase (TiC, face-centered cubic lattice, space group Fm-3m (225), PDF 04-004-2919) is present as a majority phase in the sample $M_2$(deposited at 100°C). The mean crystallites size for (200) is 6.6 nm.

In the sample $A_6$(obtained at 400°C) only face-centered cubic phases can be found. If the deposition parameters will be improved, and oxygen will be removed, only Ti-C face-centered cubic phases will be obtained, meaning that all titanium atoms will react with carbon atoms.

In the sample $B_6$(deposited at 400°C) a single polycrystalline phase is found (TiC0.4O0.6, face-centered cubic lattice, space group Fm-3m (225), PDF 04-021-7421). We used Williamson-Hall formula for the determination of the mean crystallite size (D). The microstrain (η) for the TiC0.4O0.6 phase was also computed.

The obtained values are D = 15.5 nm and η = 0.08 %. The thickness of this sample is 100 nm, according to the XRR measurements. Surprisingly, in the sample $B_1$ (deposited at room temperature) there is present a high concentration (40%) of TiC0.921 (face-centered cubic lattice, space group Fm-3m (225), PDF 04-002-5601). In this case, the mean crystallite size for (200) is 7.1 nm.

The most promising route to obtain c-TiC as a single phase, seems to be the co-deposition at 400 °C, if oxygen will be removed.

The tribological measurements highlighted a decrease of the friction coefficient with the increase of the normal load. We suppose the measured values of friction coefficient are associated with the occurrence of atomic diffusion process at Ti/C interface and with the appearance of $Ti_xC_y$ phases.

Electrical surface resistance was measured at different temperatures comparing the voltage drop on the sample studied with the voltage drop on a standard series resistance.

The electrical conductivity decrease with the increase of the temperature in the case of sample *A2* and increase with increase of the temperature in the case of sample *B1*.

Based on Wiedemann-Franz law the thermal conductivity was calculated using electrical conductivity. So it can be seen that such structures are good thermal isolators.

## REFERENCES

[1] [Kim, H.S.; Yoo, S.J.; Ahn, J.W.; Kim, D.H.; Kim, W.J.. Mater. Sci. Eng. A 2011, 528, 8479–8485.
[2] Bai, W.Q.; Li, L.L.; Wang, X.L.; He, F.F.; Liu, D.G.; Jin, G.; Tu, J.P. Surf. Coat. Technol. 2015, 266, 70–78.
[3] Caschera, D.; Federici, F.; Pandolfi, L.; Kaciulis, S.; Sebastiani, M.; Bemporad, E.; Padeletti, G. Thin Solid Films 2011, 519, 3061–3067.
[4] Oláh N, Cora I, Horváth Z, Csanádi T, Sulyok A and Balazsi K 2018 Journal of the European Ceramic Society **38** 2886
[5] Rubshtein A P, Vladimirov A B, Korkh Y V, Ponosov Y and Plotnikov S A 2016 Surface and Coatings Technology **309** 680
[6] Kaipoldayev O E, Baigarinova G A, Nemkayeva R R, Guseinov N R, Mukhametkarimov Y S, Tauasarov K and Prikhodko O Y 2019 Journal of Nano- and Electronic Physics **11** 4001
[7] Oláh N, Cora I, Horváth Z, Csanádi T, Sulyok A and Balazsi K 2018 Journal of the European Ceramic Society **38** 2886
[8] Zhou B, Liu Z, Rogachev A V, Piliptsou D G and Tang B 2016 Surf. and Interface Analysis **49** 47
[9] Hong Z-C, Hsueh H-C, Wu C-Z and Shiue S-T 2018 Thin Solid Films **660** 899
[10] Liu X, Liu L, Sun B, Li B and Ke X 2016 J. of Measurements in Engineering **4** 167
[11] Zábranský L, Buršíková V, Souček P, Vašina P, Gardelka T, Sťahel P, Caha O, Peřina V and Buršík J 2014 Surface and Coatings Technology **242** 62
[12] Rubshtein A P, Vladimirov A B, Plotnikov S A, 2018, Solid State Phenomena **279** 153
[13] Bai W Q, Li L, Wang X, He F F, Liu D, Jin G and Tu J P 2015 Surface and Coatings Technology **266** 70
[14] Dwivedi N, Kumar S and Malik H K 2011 ACS Applied Materials & Interfaces **3** 4268
[15] Zhang S, Yan M, Yang Y, Zhang Y, Yan F and Li H 2019 Carbon **151** 136
[16] Torskaya E, Mezrin A and Sánchez-López J C 2019 Proc. of the 4th Int. Conf. on Industrial Engineering (Moscow) vol 0 (Springer, Cham) p 1003
[17] Torskaya E, Mezrin A and Sánchez-López J C 2019 Proc. of the 4th Int. Conf. on Industrial Engineering (Moscow) vol 0 (Springer, Cham) p 1011
[18] Vladoiu, R.; Tichý, M.; Mandes, A.; Dinca-Balan, V.; Kudrna, P. Coatings **2020**, 10, 211
[19] Vladoiu, R.; Ciupina, V.; Mandes, A.; Dinca, V.; Prodan, M.; Musa, G. J. Appl. Phys. 2010, 108, 093301.
[20] Lungu, C.P.; Mustata, I.; Musa, G.; Lungu, A.M.; Brinza, O.; Moldovan, C.; Rotaru, C.; Iosub, R.; Sava, F.; Popescu, M.; et al. J. Optoelectron. Adv. Mater. 2006, 8, 74–77.

[21] Ciupina, V.; Vladoiu, R.; Lungu, C.P.; Dinca, V.; Contulov, M.; Mandes, A.; Popov, P.; Prodan, G. Eur. Phys. J. D 2012, 66, 99.
[22] Vladoiu, R.; Dinca, V.; Musa, G. Eur. Phys. J. D 2009, 54, 433–437.
[23] Musa, G.; Vladoiu, R.; Ciupina, V.; Janick, J. J. Optoelectron. Adv. Mater. 2006, 8, 621–623.
[24] Vladoiu, R.; Mandes, A.; Dinca, V.; Balasoiu, M.; Soloviov, D.; Turchenko, V. *Materials* 2020, *13*, 399.
[25] Ciupina, V, Lungu, Vladoiu, R Porosnicu, C, Vasile, E, Nicolescu, V, Mandes, A, Dinca, V, Cupsa, O PHYSICA SCRIPTA Vol.: 95 Issue: 4 Article Number: 044012, 2020
[26] V. Ciupina, C. P. Lungu, E. Vasile, G. Prodan, C, Porosnicu R. Vladoiu et al., J. of Ovonic Research, Vol. 18, Issue 2, Page 177-186
[27] V. Ciupina, C. P. Lungu, R. Vladoiu, G. Prodan, C, Porosnicu, et al., Book Series: Proceedings of SPIE NANOSTRUCTURED THIN FILMS XVII, 2019, Volume: 11089, Article Number: UNSP 110890N, DOI: 10.1117/12.2528663, ISBN:978-1-62841-724-1, ISSN: 0277-786X
[28] V. Ciupina, C. P. Lungu, E. Vasile, G. Prodan, C, Porosnicu R. Vladoiu, et al., Titanium - Carbon Multilayer Nanostructures Obtained by Thermionic Vacuum Arc Method, AIP Conference Proceedings, Conference TURKISH PHYSICAL SOCIETY Volume: 2178, Article Number: 030035, DOI: 10.1063/1.5135433, 35TH INTERNATIONAL PHYSICS CONGRESS (TPS35), SEP 04-08, Bodrum, TURKEY, 2019
[29] Schwan J, Ulrich S, Batori V and Ehrhardt H 1996 Journal of Applied Physics 80 440
[30] MINCRYST (khamrabaevite-7200)